

# JP1J.17 ASSIMILATION OF MULTIPLE-DOPPLER RADAR DATA WITH WRF-3DVAR SYSTEM: PRELIMINARY RESULTS IN OBSERVING SYSTEM SIMULATION EXPERIMENTS

Soichiro Sugimoto\*<sup>1,2</sup>, N. Andrew Crook<sup>2</sup>, Juanzhen Sun<sup>2</sup>, Dale M. Barker<sup>2</sup>, and Qingnong Xiao<sup>2</sup>

1. Central Research Institute of Electric Power Industry, Abiko, Chiba, JAPAN

2. National Center for Atmospheric Research, Boulder, Colorado, USA

## 1. INTRODUCTION

Dynamic and microphysical retrieval at the convective scale is a great challenge for quantitative precipitation forecasting of convective weather. Doppler radar provides an unrivalled data source of convective fields at high spatial and temporal resolution. The use of four-dimensional variational data assimilation (4DVAR) with radar data has been demonstrated to be promising (Sun and Crook (1998)) and seems to be most accurate for the retrieval.

However, application of 4DVAR data assimilation to a large domain requires huge computational resources and is not likely easy to implement under an operational environment. During the past few years, the development of a 3DVAR system, designed for the Weather and Research Forecast (WRF) model (Skamarock *et al.* (2005)), has been accelerated. The WRF-3DVAR could play an important role as a tool for its application and research of radar data assimilation.

The main objective of this study is to evaluate the capability of WRF-3DVAR for assimilating radar data (radial velocity data and reflectivity factor data) to recover the three-dimensional wind, temperature, and moisture fields. Then, Observing System Simulation Experiments (OSSEs) are performed with simulated observations. Another aim is the use of a cloud analysis scheme to help inserting or removing convection is tested.

## 2. FUNCTION OF 3DVAR IN WRF-VAR SYSTEM

### 2.1 Overview

The WRF-VAR is a newly developed variational

data assimilation system, which is designed for the WRF model. There was a major update from the previous version of WRF-3DVAR that originates and evolves from MM5-3DVAR. The basic interface is fully consistent with the WRF model, and it will provide capability for 4DVAR. Some significant improvements have been also achieved in WRF-VAR 3DVAR as described in Skamarock *et al.* (2005). Barker *et al.* (2003) and Barker *et al.* (2004) describe in detail the 3DVAR algorithm. Here, a few explanations are given to help understanding this study.

A cost function is defined to measure the difference between the model and observations.

$$J(\mathbf{x}) = \frac{1}{2}(\mathbf{x} - \mathbf{x}_b)^T \mathbf{B}^{-1}(\mathbf{x} - \mathbf{x}_b) + (\mathbf{y} - \mathbf{y}^o)^T \mathbf{R}^{-1}(\mathbf{y} - \mathbf{y}^o), (1)$$

where

$\mathbf{x}$  is a vector of analysis,

$\mathbf{x}_b$  is a vector of background (first-guess),

$\mathbf{B}$  is the background error covariance matrix,

$\mathbf{y}^o$  is a vector of observation,

$\mathbf{y}$  is a vector of model-derived observation transformed by the observation operator  $H$  ( $\mathbf{y}=H(\mathbf{x})$ ), and

$\mathbf{R}$  is the observational and representativeness error covariance matrix.

The incremental cost function is derived by preconditioning via a control variable transformation  $\mathbf{x}-\mathbf{x}_b=\mathbf{U}\mathbf{v}$ , where  $\mathbf{v}$  is a vector of control variable. This preconditioning means that the background error covariance  $\mathbf{B}$  is equivalent to  $\mathbf{U}\mathbf{U}^T$  if  $\mathbf{U}$  is well designed. Practically, the control variable transform is performed by a series of operations  $\mathbf{U}=\mathbf{U}_p\mathbf{U}_v\mathbf{U}_h$ , where  $\mathbf{U}_h$  is the horizontal transform by recursive filters,  $\mathbf{U}_v$  the vertical transform via an empirical orthogonal function (EOF) decomposition, and  $\mathbf{U}_p$  the physical variable transformation involving the conservation of control variables to model variables increments. A method to estimate three components of the control variable transformation is noted in section 3.3. This study uses the conjugate gradient method to minimize the incremental cost function.

---

\*Corresponding author: Soichiro Sugimoto, Central Research Institute of Electric Power Industry, 1646 Abiko, Abiko, Chiba 270-1194, Japan; E-mail: soichiro@criepi.denken.or.jp, or sugimoto@ucar.edu

The above preconditioning serves to compute  $\mathbf{B}^{-1}$  efficiently under an assumption that error correlations among control variables are uncorrelated. In the case of assimilating only radial velocity data, streamfunction, unbalanced velocity potential, unbalanced temperature, pseudo relative humidity, and unbalanced surface pressure are used as control variables. In the case of additional assimilation of reflectivity factor, the total water mixing ratio (sum of water vapor, cloud water, and rainwater) is used as a moisture control variable instead of pseudo relative humidity.

## 2.2 Assimilation of Radial Velocity Data

Radial velocity  $V_r$  is defined using wind components ( $u, v, w$ ), vertical fallspeed of hydrometeor (currently related only with rainwater)  $V_t$ , and distance  $R$  between locations of radar site and data point:

$$V_r = \frac{1}{R} \{ (x - x_R)u + (y - y_R)v + (z - z_R)(w - V_t) \}, \quad (2)$$

$$R = \sqrt{(x - x_R)^2 + (y - y_R)^2 + (z - z_R)^2}, \quad (3)$$

where  $(x, y, z)$  represent the location of radar data and  $(x_R, y_R, z_R)$  the location of a radar site. Vertical fallspeed  $V_t$  is calculated from the rainwater mixing ratio  $q_r$  with height correction (Sun and Crook (1997)).

Model-derived radial velocities are based on this operator. Observed radial velocities are also simulated using this operator in our OSSEs. The details will be described in section 3.2.

## 2.3 Assimilation of Reflectivity Factor Data

The following equation is used as a relationship between rainwater mixing ratio and reflectivity factor.

$$Z = 43.1 + 17.5 \log(\rho q_r), \quad (4)$$

where  $Z$  is reflectivity factor in the units of dBZ, and  $\rho$  is the air density. This is derived assuming the Marshall-Palmer type of drop size distribution and reflectivity factor contributed only by rainwater (without ice phases). Reflectivity factor is directly assimilated so that model-derived reflectivity factor is calculated with Equation (4) in the cost function of Equation (1). Observed reflectivity factor in OSSEs is based on this operator as well.

As noted in section 2.1, the total water mixing ratio is used as a moisture control variable. Therefore, we need to introduce a partitioning method in the physical variable transformation  $\mathbf{U}_p$ . Four processes; condensation, autoconversion, accretion, and evaporation are considered in a warm rain regime. Isobaric process is assumed for transformation between water vapor and cloud water in condensation process. We used the same empirical equations as the ones used in Sun and Crook (1997) for the remaining processes.

Some difficulty arises if the background has no convection but there is rainfall indicated by radar. Since radar indicates the existence of precipitation in the atmosphere but gives no information about temperature and water vapor fields, it is challenging to insert or remove convection in the framework of 3DVAR. In this study, the use of a cloud analysis scheme is tested to make the new background for 3DVAR using the original background.

First of all, a budget analysis of rainwater on each grid point with equation (5) is performed to estimate model-derived latent heating as well as observation-derived latent heating.

$$u \frac{\partial q_r}{\partial x} + v \frac{\partial q_r}{\partial y} + w \frac{\partial q_r}{\partial z} - \frac{\partial (V_t q_r)}{\partial z} = Q, \quad (5)$$

where  $Q$  is source and sink term of rainwater. Here, we assume to have observation-derived rainwater in the model space by geometrical interpolation. This interpolation is only for the cloud analysis. Of course, no geometrical transformation is needed for any observations in 3DVAR. Then, the difference of latent heating between the two fields is estimated from the difference of  $Q$ , and it is inserted into the “background” field to modify temperature.

Second, observation-derived latent heating is used to determine if the air is saturated (that is positive latent heat). If the air is not saturated, cloud water mixing ratio in the background is set to be zero, and humidity is modified to be a threshold when humidity is greater than the threshold (e.g., 70 %). Details of the method will be described at the presentation.

Third, analysis with 3DVAR is performed using the modified background. A combined use of the cloud analysis and 3DVAR is iterated at several times. Such iteration is called the “outer-loop” in the WRF-VAR.

### 3. SETUP OF OSSEs

#### 3.1 Experimental Design

Assimilation with WRF-3DVAR requires both a background field plus observations (see equation (1)). In our OSSEs, results from two different simulations with the WRF model are used for making the background and observations. The only difference of configuration between two WRF simulations is the time of the initial and boundary conditions.

First of all, we define a “background” field and a “true” field. Then, the “background” field is prepared as a forecast from one control simulation with the initial and boundary conditions at 1200Z, June 12, 2002. The forecast will be also referred to as the results of a case study called “no assimilation”. Meanwhile, the “true” field is prepared as a forecast from another simulation which is initiated at a different time (1500Z, June 12, 2002). The “true” field is used for making radar observations with the operators described in the previous section. Simulated radar observations are assimilated into the “background” field with 3DVAR.

We perform OSSEs at the cold-start mode and the cycling-mode for radial velocity assimilation at first. Then, idealized data (see section 3.2) are used for the cold-start mode 3DVAR to evaluate maximum potential of assimilation. For the cycling-mode 3DVAR, observations are assimilated at intervals of 1 hour, 30 minutes, or 15 minutes from 2100Z, June 12 to 0000Z, June 13. Only radial velocity data are assimilated for the cycling mode 3DVAR, and data are limited within a storm region. Next, the cold-start mode 3DVAR using radial velocity data within a storm is applied to two different timings to evaluate its impact on precipitation forecasting. As a final experiment, reflectivity factor assimilation is tested with the cold-start mode. Experiments are summarized below.

Experiment 1: Radial velocity assimilation (at 0000Z with idealized data). Evaluation of the wind retrieval.

Experiment 2: Radial velocity assimilation (2100Z to 0000Z at 1-hr, 30-min, or 15-min interval with storm data). Evaluation of the wind retrieval.

Experiment 3: Radial velocity assimilation (at 2100Z or 0000Z with storm data). Evaluation of precipitation forecasting.

Experiment 4: Additional assimilation of reflectivity factor (at 0000Z with storm data). Evaluation of the retrieval of moisture variables and temperature, and precipitation forecasting.

#### 3.2 Simulated Observations and Their Errors

The actual WSR-88D network is considered, and radar observations are simulated for 25 radar sites in a domain for simulations with the WRF model (Figure 1). The domain has horizontal grid spacing of 4 km, and 36 full sigma levels are contained in the vertical. It is noted that no spatial interpolation from radar observation space to model grid space or vice versa is performed, because the calculation of radar observations is done for each model grid point.

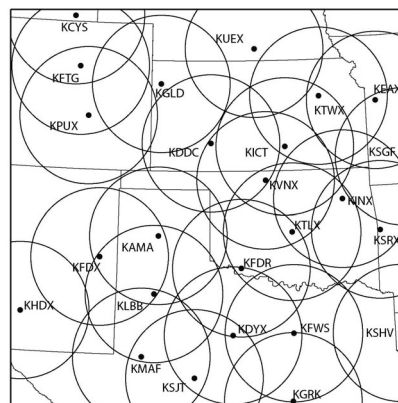


Figure 1: Model domain and the WSR-88D radar sites together with the radar coverage (circles).

Though the actual radar beam pattern and observation range (200 km radius for each) are considered, radar observations are assumed to be obtained at all model grid points within the radar coverage for Experiment 1. It is an idealized situation for evaluation of maximum potential of radial velocity assimilation. The total number of radial velocity observations to be assimilated is about 6 million in this experiment. In the remainder of experiments, lowest detectable levels are set to be 20 dBZ for reflectivity factor observations and 5 dBZ for radial velocity observations to limit data within a storm.

The error in radial velocity is assumed to have an unbiased normal distribution (standard deviation of  $1 \text{ m s}^{-1}$ ) is calculated using Box-Muller transformation as a random number generator. To avoid an excessively large weighting of data, any absolute value of error

smaller than  $0.5 \text{ m s}^{-1}$  is set to be  $0.5 \text{ m s}^{-1}$ . For reflectivity factor, the same setting as above is adopted except for the units of dBZ.

### 3.3 Estimation of Background Error Statistics

The performance of a VAR system largely depends on the plausibility of the background error covariance matrix  $\mathbf{B}$  in equation (1). The matrix contains important information about how the impact of assimilating an observation spreads in the model space and about how the final analysis is physically balanced. The fact that we cannot know the true state of the atmosphere makes the estimation of the matrix too difficult.

It seems that the use of results from ensemble forecasts or application of ensemble Kalman filter are promising methods, but further investigation is still needed. In this study, a statistical analysis via the NMC method (Parrish and Derber (1992)) is used for a case-specified matrix with a series of ten 1-day-forecasts which are performed every 12-hrs from 10 June, 2002 to 14 June, 2002. Then, each 12-hrs forecast is compared with 24-hrs forecast for the same time to estimate statistics. This is a crude but straightforward approach. Note that the time/domain averaged estimates are used in this study.

The NMC method provides mainly three estimates for WRF-3DVAR as follows:

- Eigenvectors/eigenvalues of the vertical component of  $\mathbf{U}_v$
- The recursive filter's characteristic lengthscale for each control variable and for each vertical mode (used for  $\mathbf{U}_h$ )
- Regression coefficient to calculate the total part of variable from the unbalanced part of variable (used for  $\mathbf{U}_p$ )

Eigenvectors/eigenvalues and lengthscale are tuned for more reasonable results because the time lag between WRF simulations for the "background" and "true" fields is 3 hours which is shorter than 12 hours.

### 3.4 Comparison with Two Simulations for a Convective Storm Event

As noted above, the same setup of the WRF model is used for two different model simulations. First of all, the WRF model version 2.0.3.1 is used. The setup for the model domain is described in section 3.2. The

model top is located at 50 hPa. Analyses from NCEP's Eta Data Assimilation System (EDAS) are used as the initial and boundary conditions. The model is integrated with a time step of 20 seconds (5 seconds for the acoustic wave) without any diffusion scheme. The configuration for parameterization of dynamical and microphysical processes is listed as follows:

- Surface model: Noah Land Surface Model
- Planetary boundary layer: YSU Model
- Cumulus scheme: None
- Microphysics: WRF Single Moment Model 6 (WSM6)

Our OSSEs are performed for a dryline case that occurred over the Southern Great Plains. Plots of the 1-h accumulated precipitation from 2100Z, June 12 to 0300Z, June 13, 2002 for the background and truth simulations are compared in Figure 2. In the "true" field, convection is initiated along a dryline at 2100Z. However, there is no significant convection in the same region for the "background" field. Another big difference between forecasts at 2100Z is found in the north-east corner of Oklahoma. Convection developed in the "background" field is not significant in the "true" field. Forecasts in later hours indicate clear differences in the evolution and the movement of precipitation area. The differences are caused only by a 3-h time lag of initial time, which motivates us to assimilate radar observations so that the location, timing, and evolution of convection in later hours are improved.

## 4. RESULTS

### 4.1 Maximum Potential of Radial Velocity Assimilation for Wind Retrieval (Experiment 1)

Throughout this study, observations are simulated from the "true" field and assimilated. Therefore, key features found in "Observation minus Background (O-B)" innovation are retrieved in "Analysis minus Background (A-B)" increment if the framework of radial velocity assimilation is well designed. Good performance also means that the root mean square (RMS) error in "Analysis minus Observation (A-O)" residual becomes smaller than the RMS error in O-B. Furthermore, positive impacts on precipitation forecasting are also expected after 3DVAR analysis.

Figures 3, 4, and 5 are comparisons for Experiment 1 between O-B and A-B at the model level

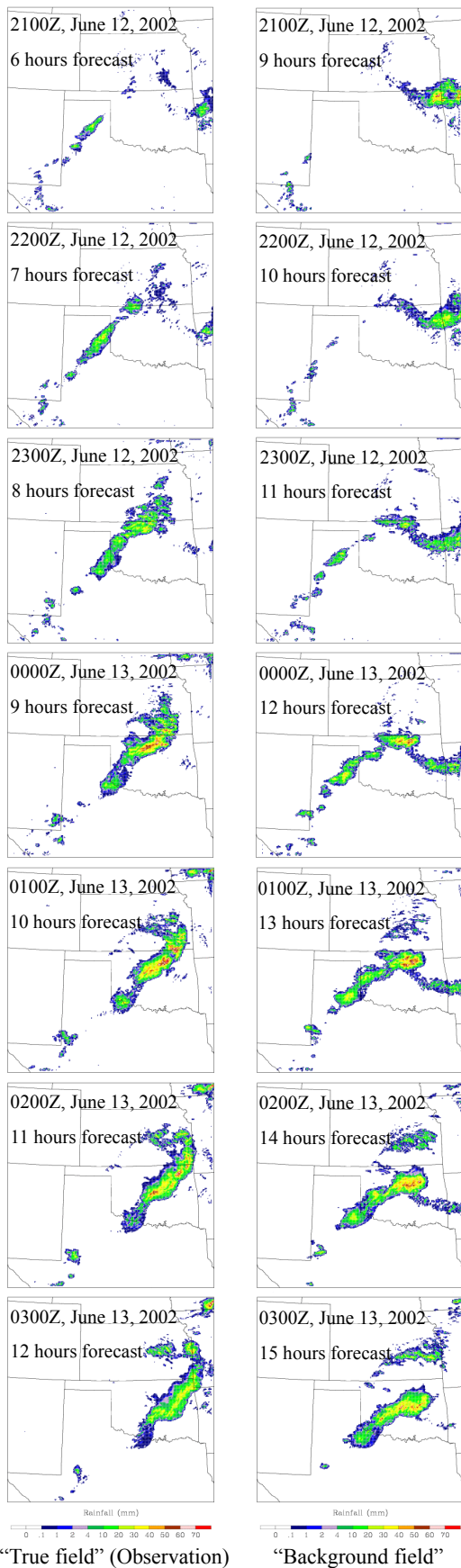


Figure 2: 1-h accumulated precipitation by two different simulations (left: the “true” field; right: the “background” field or “no-assimilation” case).

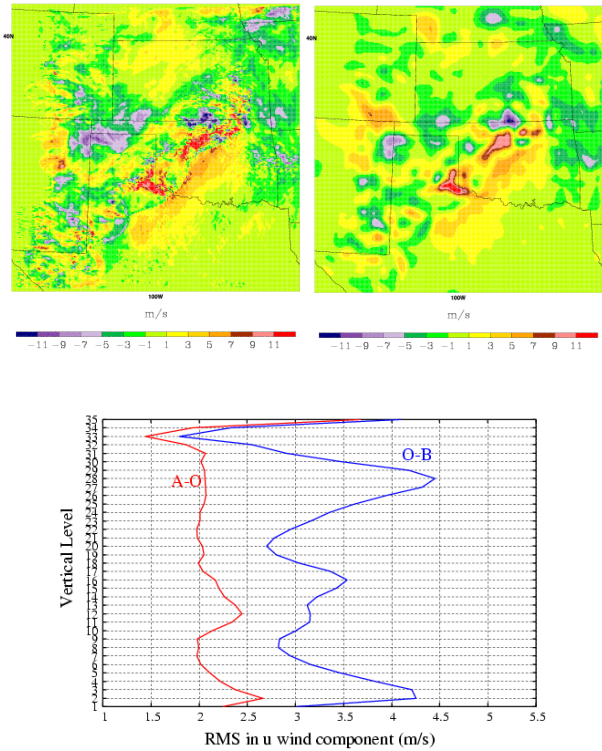


Figure 3: Retrieval of u-wind component at the model level of 10 (Experiment 1 at 0000Z, June 13, 2002) [upper-left: Observation minus Background (O-B), upper-right: Analysis minus Background (A-B), lower: RMS error for each level].

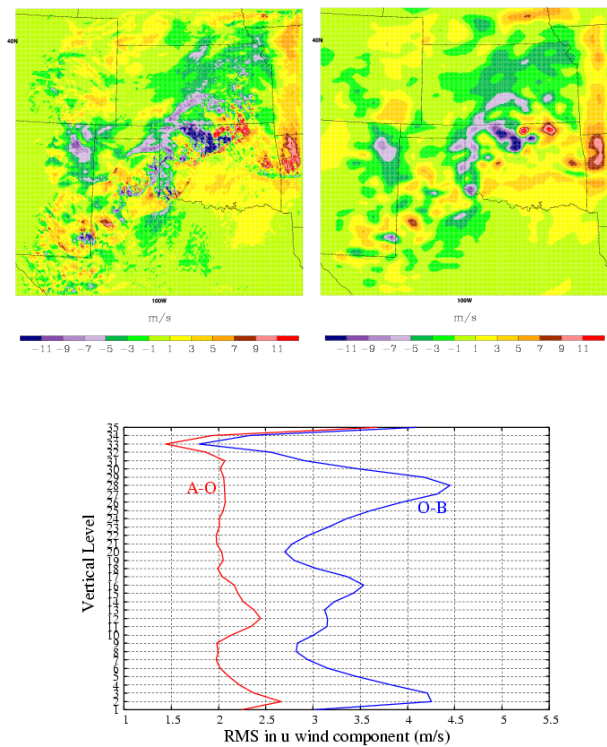


Figure 4: Similar to Figure 3, but for v-component.

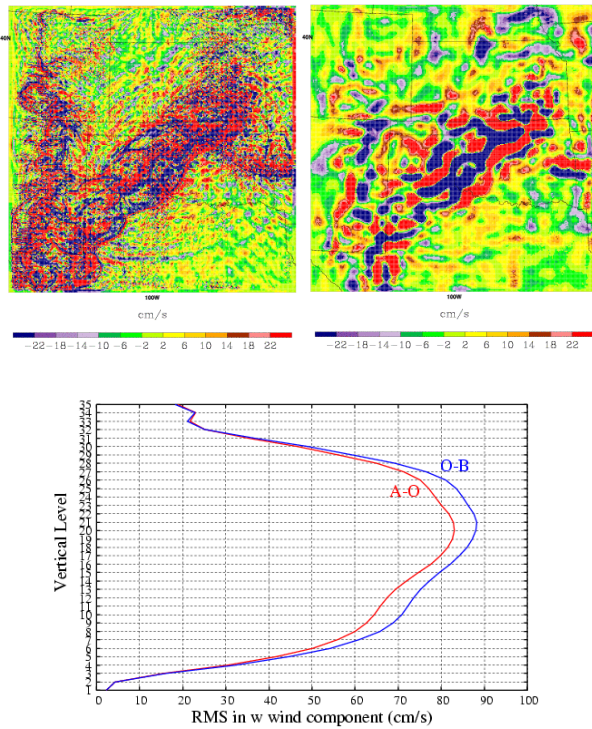


Figure 5: Similar to Figure3, but for w-component.

level of 10 for u-, v-, and w-component, respectively. The RMS errors in O-B (blue line) and A-O (red line) for each vertical level are also plotted. Generally, the positive impact is demonstrated in the profile of the A-O RMS error. The score is improved by several percent from the result (Sugimoto *et al.* (2005)) with the previous version of WRF-3DVAR. The horizontal winds are appropriately recovered by the radial velocity assimilation. The retrieval is achieved at scales larger than the convective scale. This is clearly shown in the vertical velocity field in Figure 5. Note that the convective-scale structure in O-B is considerably smoothed in O-A. These results suggest that a sophisticated dynamical framework with the use of flow-dependent background error statistics will be needed for the successful wind retrieval at the convective scale.

#### 4.2 Effects of Using the Cycling Mode 3DVAR (Experiment 2)

The maximum performance of radial velocity assimilation with WRF-3DVAR is found in the previous experiment. The performance evaluated, however, would be degraded for assimilation with real data because less data is available due to the detectable level of a radar system. Since one of the advantages

of radar observations is that data can be obtained with a high temporal resolution (e.g. 5 minutes), the use of the cycling mode 3DVAR is considered.

Benefits of the cycling mode are evaluated from the temporal change of the RMS error of v-wind component. Figure 6 shows the RMS errors in the cases of “no-assimilation” and “assimilation” for each cycling interval. The RMS error is averaged within a storm region. Generally, the error increases as time progresses for “no-assimilation” case. Each of assimilation cycles reduces the RMS error and prevents the rapid increase of the error. As more rapid

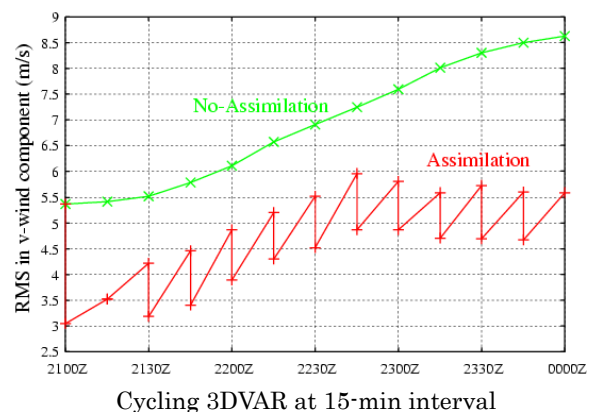
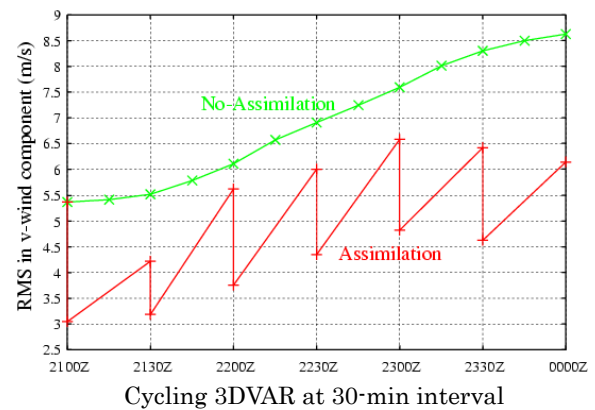
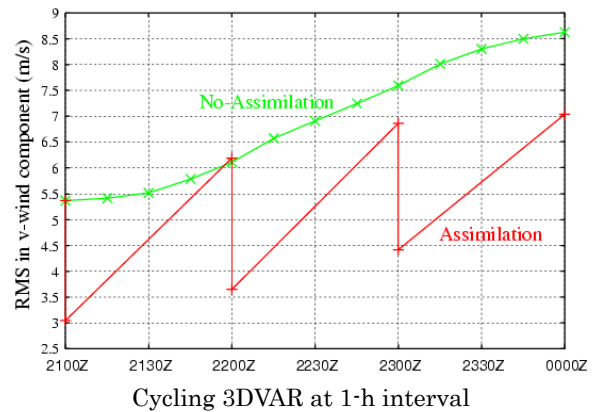


Figure 6: Temporal variation of the RMS error in v-component wind (Top: 1-h interval, Middle: 30-min interval, Bottom: 15-min interval).

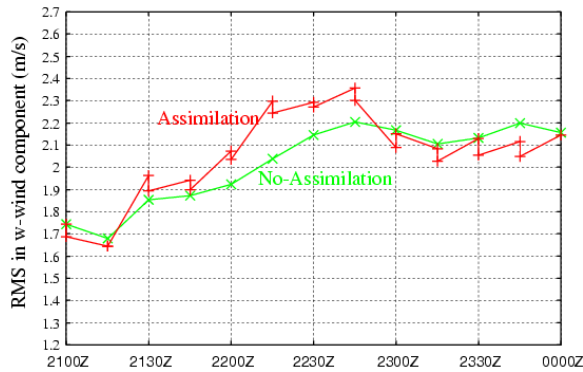


Figure 7: Temporal variation of the RMS error in w-component wind (15-min interval).

cycle is used, the error is more effectively reduced.

It is interesting that a response after assimilation differs somewhat according to the evolution stage of convection. The accuracy is kept within the 30-min time window from 2100Z, but it is gradually degraded after 2130Z up to 2300Z. After 2300Z, the accuracy is actually improved as assimilation is performed for the cycling mode 3DVAR at 15-min interval.

Figure 7, which shows temporal variation of the RMS error of the vertical wind component, suggests the possible reason of degradation within a time window from 2130Z to 2300Z. Clearly, the RMS error increases during the time window. This suggests that the retrieval of the vertical wind at the convective scale is needed to be improved especially when the stage of convection is developing.

#### 4.3 Impact of Radial Velocity Assimilation on Precipitation Forecasting (Experiment 3)

Figure 8 shows the 1-h accumulated precipitation forecasted with the final analysis by the cold-start mode 3DVAR at 2100Z, together with observations from the “true” field. Positive impacts are found in 1-h, 2-hrs, and 3-hrs forecasts. Deficiencies in the background field at 2100Z, which are pointed out in section 3.4, are modified so that the location and timing of convection initiated along the dryline are forecasted better.

However, improvements of the wind field are less effective for precipitation forecasting in the case of the cold-start 3DVAR at 0000Z (Figure 9). Only a slight modification is found up to 2-hrs after assimilation. Convection along the dryline is also forecasted a little better, but benefits are dissipated by convection which originally existed in the background.

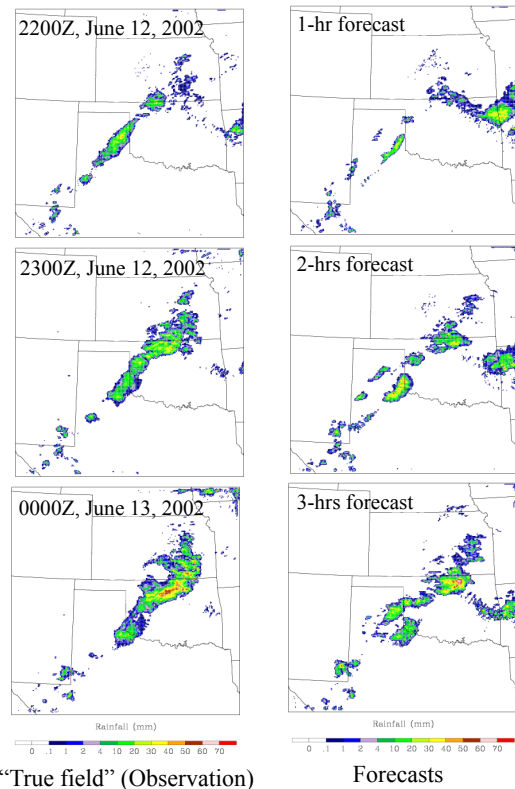


Figure 8: 1-h accumulated precipitation forecasted with the final analysis at 2100Z (left: observations (the “true” field); right: forecasts).

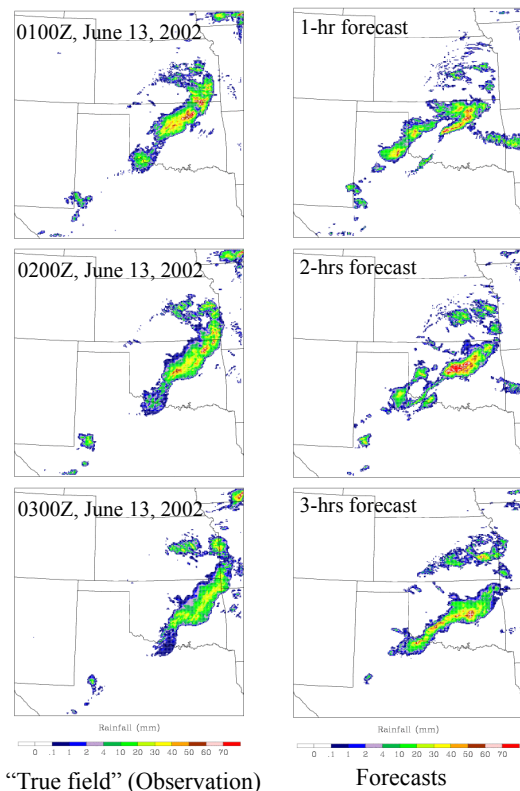


Figure 9: 1-h accumulated precipitation forecasted with the final analysis at 0000Z (left: observation (the “true” field); right: forecasts).

The result from assimilation at 2100Z indicates that assimilating radial wind observations can serve for triggering convection. In other words, the location of convergence along the dryline is relatively important. Once convection is developed, the retrieval of water vapor and temperature fields is probably crucial to control convective activity.

#### 4.4 Preliminary Result of Reflectivity Factor Assimilation (Experiment 4)

Figure 10, 11, 12, and 13 show comparisons between O-B and A-B for rainwater, cloud water, water vapor, and temperature, respectively. Other than rainwater, all variables are unobserved. Note that A-B is affected by 3DVAR as well as the cloud analysis scheme. First of all, rainwater is recovered appropriately. Next, pattern of negative value of cloud water in A-B corresponds well in the pattern in O-B. This is due to the cloud analysis. However, positive value along the dryline cannot be recovered satisfactorily. The reason is probably because radar data are available mainly in the north side of the dryline, but positive value is found just along the dryline. Retrieval of temperature field is achieved fairly well. Cooling by evaporation in an area of heavy precipitation is important in this case and recovered. Finally, water vapor is mainly modified by the cloud analysis and the modification is appropriate. However, there is still a problem in the lower atmosphere.

Result of precipitation forecasting with the analyzed field is shown in Figure 13. Compared with the result from radial velocity assimilation (Figure 9), shape and evolution of convection are significantly improved. This encourages us to develop a methodology in which 3DVAR is performed iteratively together with a cloud analysis.

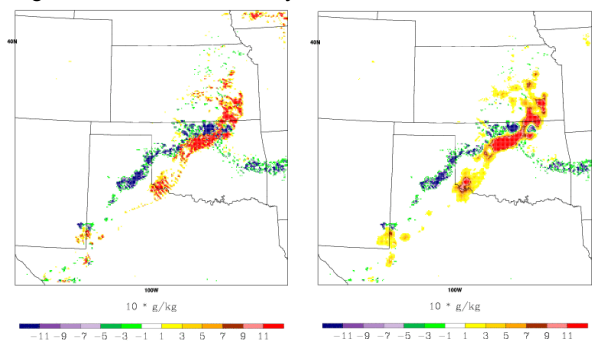


Figure 10: Retrieval of rainwater [left: Observation minus Background (O-B), right: Analysis minus Background (A-B)].

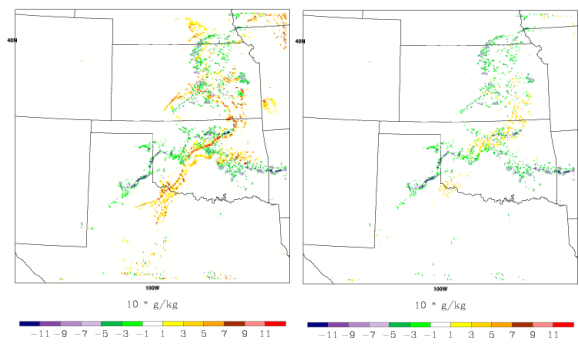


Figure 11: Retrieval of cloud water [left: Observation minus Background (O-B), right: Analysis minus Background (A-B)].

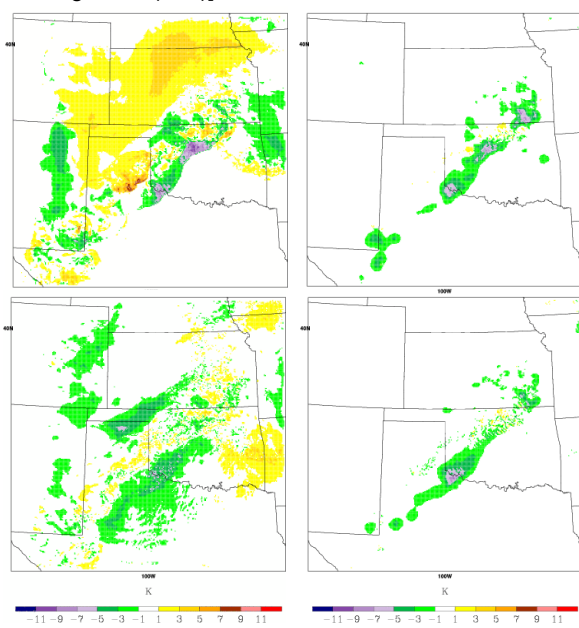


Figure 11: Retrieval of temperature [left: O-B, right: A-B, upper: level 6, lower: level 12].

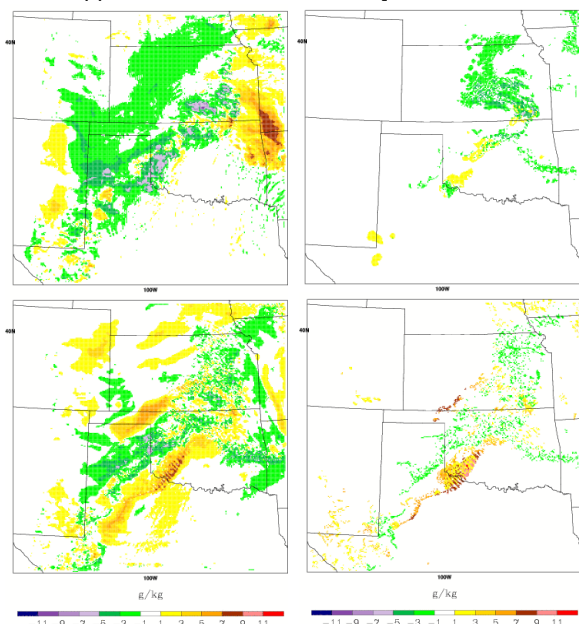


Figure 12: Retrieval of temperature [left: O-B, right: A-B, upper: level 6, lower: level 12].

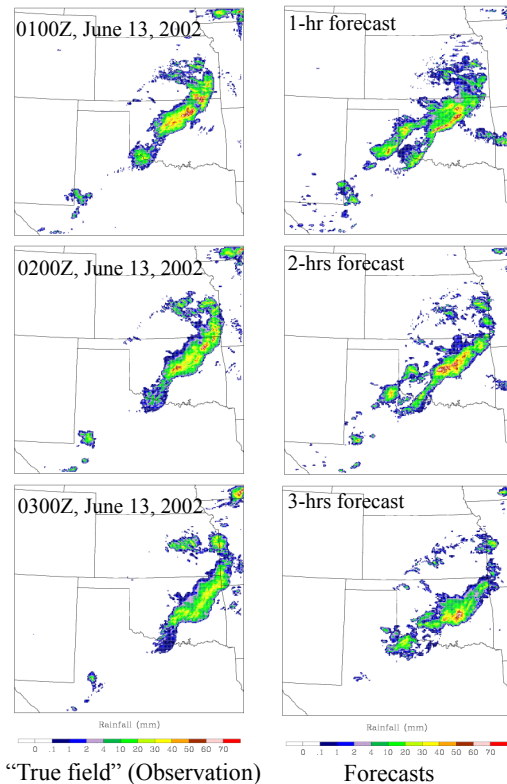


Figure 13: 1-h accumulated precipitation forecasted with the final analysis at 0000Z (left: observation (the “true” field); right: forecasts).

## 5. SUMMARY

This study investigates the performance of radar data assimilation in terms of the retrieval of convective fields and its impact on precipitation forecasting. The investigation is done with WRF-VAR 3DVAR system via several OSSEs.

Results for the cold-start 3DVAR mode with idealized radial velocity data indicates that the radial velocity assimilation works reasonably well in recovering the key feature of the wind field at scales relatively larger than the convective scale. However, a more sophisticated dynamical framework with a flow-dependent background error statistics will be needed for the retrieval at the convective scale.

The use of the cycling mode 3DVAR serves to prevent the model error increasing rapidly with time. This encourages using radar observations with a high temporal resolution. At least, the interval of 15 minutes likely works well for radial velocity assimilation. Result indicates the need of more accurate retrieval of the vertical wind component.

Positive impact on precipitation forecasting is

found from results of OSSEs with radial velocity within a storm region. It is apparent if the convection is in the initiation stage. The impact lasts for about 3 hours after assimilation. Meanwhile, benefits of radial velocity assimilation on precipitation forecasting are less for convection in the developing or the mature stage.

Such a situation is significantly improved by the additional assimilation of reflectivity factor. Preliminary result suggests that the combined use of 3DVAR and a cloud analysis works to some extent for the retrieval of unobserved variables even when the background has no convection.

## References

- Barker, D. M., W. Huang, Y.-R. Guo, and A. J. Bourgeois, 2003: A Three-Dimensional Variational (3DVAR) Data Assimilation System for Use with MM5. NCAR Technical Note, NCAR/TN-453+STR, 68 pp.
- Barker, D. M., W. Huang, Y.-R. Guo, A. J. Bourgeois, and Q. Xiao, 2004: A Three-Dimensional Variational Data Assimilation System for MM5: Implementation and Initial Results. *Mon. Wea. Rev.*, 132, 897-914.
- Parrish, D. F., and J. C. Derber, 1992: The National Meteorological Center’s Spectral Statistical Interpolation Analysis System. *Mon. Wea. Rev.*, 120, 1747-1763.
- Skamarock, W. C., J. B. Klemp, J. Dudhia, D. O. Gill, D. M. Barker, W. Wang, and J. G. Powers, 2005: A Description of the Advanced Research WRF Version 2. NCAR Technical Note, NCAR/TN-468+STR, 88pp.
- Sugimoto, S., N. A. Crook, J. Sun, D. M. Barker, and Q. Xiao, 2005: Potential Benefits of Multiple-Doppler Radar to Quantitative Precipitation Forecasting: Assimilation of Simulated Data Using WRF-3DVAR System. World Weather Research Program Symposium on Nowcasting and Very Short Range Forecasting, Toulouse, France.
- Sun, J., and N. A. Crook, 1997: Dynamical and Microphysical Retrieval from Doppler Radar Observations Using a Cloud Model and Its Adjoint. Part I: Model Development and Simulated Data Experiments. *J. Atmos. Sci.*, 54, 1642-1661.
- Sun, J., and N. A. Crook, 1998: Dynamical and Microphysical Retrieval from Doppler Radar Observations Using a Cloud Model and Its Adjoint. Part II: Retrieval Experiments for an Observed Florida Convective Storm. *J. Atmos. Sci.*, 55, 835-852.